Spatially varying regularization weights for one-step spectral CT with SQS

Pierre-Antoine Rodesch, Si-Mohamed Salim, Simon Rit

Spatially varying regularization weights for one-step spectral CT with SQS

Pierre-Antoine Rodesch, Salim Si-Mohamed and Simon Rit

***Abstract*—Photon-counting detectors provide spectral information for x-ray acquisitions. Taking advantage of this information currently requires iterative algorithms to reconstruct basis material CT images. One-step reconstruction is the simultaneous inversion of the spectral distortion occurring in the detector and the geometrical projection. Separable quadratic surrogate (SQS) algorithms have been applied to this one-step problem with satisfactory convergence and material separation. However, this class of method leads to numerical instabilities stemming from voxels out of the field-of-view (FOV) which need to be included in the forward model for reconstructing the FOV. We aim at improving one-step spectral CT reconstruction by investigating two possible corrections of this effect: replacing the exponential in the forward model by a linear function for negative attenuations and spatially varying regularization depending on the geometrical conditioning. We demonstrate the efficiency of the second method using experimental data acquired on a clinical prototype CT scanner with a photon-counting detector.**

I. Introduction

In spectral computed tomography (CT), one-step approaches directly decompose photon counts in basis material density volumes. This class of methods is opposed to two-step methods, in which decomposition occurs before or after tomographic reconstruction, and which are less computationally expensive. The explicit one-step modeling enables regularization of material volumes while simultaneously inverting line integrals and the spectral distortion of the detector. This provides density maps with less correlated noise and can also be applied to K-edge imaging and unconventional scanning geometries [1].

Several algorithms have been proposed to inverse the one-step forward model. A combination of separable quadratic surrogate (SQS) and Nesterov's momentum methods have proved efficient in solving the one-step reconstruction problem of spectral CT with a K-edge material map from data acquired with photon-counting detectors [2]. In SQS approaches, each voxel is updated separately by minimizing a quadratic surrogate of the cost function at each iteration. Several SQSs have been developed for one-step spectral CT [3], [4], [6]. We chose the SQS proposed by Weidinger et al. [3] combined with ordered subsets (OS) and Nesterov's momentum technique as proposed in [4].

The problem addressed in this article are artifacts originating from voxels which are not in the field-of-view (FOV) but which are iteratively updated to accurately model the forward problem. These voxels are present in axial scans (the red stripped parts in Fig. 1) and helical scans. They cannot be accurately reconstructed due to limited angle data (since they are not in the FOV) but they influence the FOV because they are traversed by rays also going through the FOV (which is why they are reconstructed) and due to three-dimensional (3D) spatial regularization. This problem has already been described in [5] for SQS applied to mono-energetic CT in a helical acquisition case. The authors proposed to use a spatially varying update step based on their geometrical conditioning, i.e., the amount of projection data contributing to each voxel (which is less for voxels outside the FOV).

We have observed the same problem in spectral CT but the observed consequences are more severe. We focus here on the case of axial CT acquisitions. Since the forward problem generally involves the exponential function, negative values in these regions quickly translate to numbers which cannot be handled numerically. Unlike Kim et al [5], this behavior is observed without OS, but OS enhance the phenomenon. A potential solution would be the initialization of the one-step reconstruction with material volumes close to the solution [4], [6], e.g., a two-step reconstruction decomposition. We also investigate solutions for these numerical instabilities using a zero initialization to avoid the difficult question of the influence of the accuracy of the initialization.

This paper investigates two corrections. The first one is the replacement in the forward model of the exponential function by a soft-exponential as proposed by Sidky et al. [7]. The second one, inspired by [5] but formulated differently, is the

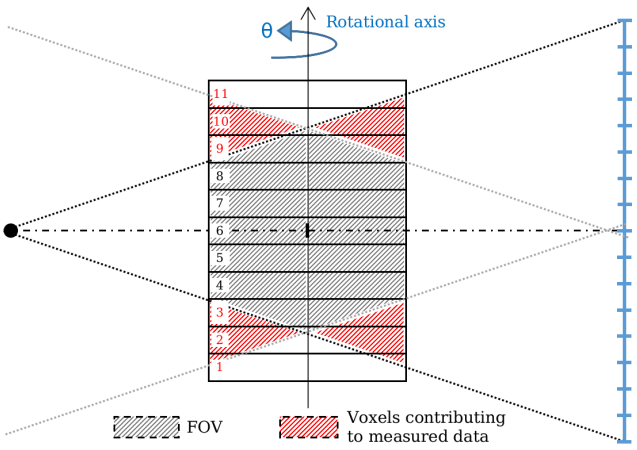

Fig. 1. Axial scan configuration with selected volume geometry. Displayed numbers correspond to slice indices used in the results section.

P.A Rodesch & S. Rit are with the Université de Lyon, CREATIS ; CNRS UMR5220 ; Inserm U1206 ; INSA-Lyon ; Université Lyon 1 ; Centre Léon Bérard, France.

Salim Si-mohamed is with the Université de Lyon, CREATIS ; CNRS UMR5220 ; Inserm U1206 ; INSA-Lyon ; Université Lyon 1, France and with the Radiology Department, Lyon University Hospital, Lyon, France.

implementation of regularization weights which vary in the volume according to the geometrical conditioning. We also study the combination of both and compare the results to the conventional SQS algorithm, with and without initialization.

II. Materials and Methods

A. SQS

We briefly summarize in this subsection common equations used in SQS techniques applied to the one-step problem. We explain the choice we made for our uncorrected method. As usual, the spectral discrete forward model is:

$$\overline{c}_{ib}(f) = \sum_{\epsilon=1}^{N_\epsilon} s_{ib}(\epsilon)\ e^{-t_i(f,\epsilon)} \tag{1}$$

where $\overline{c}_{ib}(f)$ is the expected counts in bin b for indexed detector pixel i, $s_{ib}(\epsilon)$ is the effective spectrum at energy ϵ and $t_i(f,\epsilon)$ the attenuation of the object expressed by:

$$t_i(f,\epsilon) = \sum_{m=1}^{N_m}\sum_{j=1}^{N_v} \mu_m(\epsilon) A_{ij} f_{mj} \tag{2}$$

with $\mu_m(\epsilon)$ the m-th basis (material) function, A the geometrical projection matrix and f the unknown basis volumes to be reconstructed with j the voxel index.

The problem is solved by minimizing the negative log-likelihood:

$$D_{\mathrm{PL}}(c,f) = \sum_{i=1}^{N_p}\sum_{b=1}^{N_b} \overline{c}_{ib}(f) - c_{ib}\ log\Big[\overline{c}_{ib}(f)\Big] \tag{3}$$

with c the measured photon counts.

A penalization term is added to the cost function with a spatial regularization applied independently on each basis volume:

$$R(f) = \sum_{m=1}^{N_m} \beta_m \sum_{j=1}^{N_v}\sum_{\xi\in\mathbb{V}_j}^{N_v} \phi(f_{mj} - f_{m\xi}) \tag{4}$$

with β_m the regularization weight per material and ϕ a twice differentiable convex function. In this study, we used the Green prior which, unlike others like the Huber function, does not require an extra hyperparameter. Only the β_m have to be tuned.

The SQS method for one-step reconstruction relies on the application of Newton's method at each voxel j. It enables the analytical minimization of Q^n, the SQS calculated at iteration n:

$$f_j^{n+1} = f_j^n - [H(Q^n)_j]^{-1}.[(\nabla Q^n)_j] \tag{5}$$

where $(\nabla Q^n)_j \in \mathbb{R}^{N_m}$ is the gradient of Q^n and $H(Q^n)_j \in \mathbb{R}^{N_m\times N_m}$ its Hessian. This update scheme is accelerated with OS and Nesterov's momentum technique as described by Kim et al. [8]. The gradient of the surrogate of the data fidelity term is:

$$(\nabla Q^n)_j = \sum_{i=1}^{N_p} A_{ij}\times \sum_{b=1}^{N_b}\Big(1 - \frac{c_{ib}}{\overline{c}_{ib}(f^n)}\Big)\sum_{\epsilon=1}^{N_\epsilon} s_{ib}(\epsilon) e^{-t_i(f^n,\epsilon)}\mu(\epsilon) \tag{6}$$

where $\mu(\epsilon) \in \mathbb{R}^{N_m}$ is the vector of attenuation coefficient at energy ϵ. Note that by definition of surrogates, $(\nabla Q^n) = (\nabla D_{\mathrm{PL}|f=f^n})$.

The Hessian of Weidinger's surrogate [3] is:

$$H(Q^n)_j = \sum_{i=1}^{N_p} A_{ij}\Big(\sum_{\xi=1}^{N_v} A_{i\xi}\Big)\times \sum_{b=1}^{N_b}\sum_{\epsilon=1}^{N_\epsilon} s_{ib}(\epsilon) e^{-t_i(f^n,\epsilon)}\ {}^T\mu(\epsilon)\otimes\mu(\epsilon) \tag{7}$$

where ${}^T\mu(\epsilon)\otimes\mu(\epsilon) \in \mathbb{R}^{N_m\times N_m}$.

As each basis material is regularized separately, we can directly apply the regularization surrogate of De Pierro [9] demonstrated in a mono-energetic case.

B. Proposed corrections

We now introduce modifications of the method described in the previous subsection. We investigated two solutions in order to stabilize voxels outside the FOV.

1) *Soft-exponential (Soft-E)*: Even though negative values of attenuation $t_i(f,\epsilon)$ are unphysical, they can occur, in particular in early iterations. The calculation of an exponential on a positive number will produce large gradient values causing divergence. To counteract this effect, we investigated the use of the (negative) soft-exponential (adapted from Sidky et al. [7]):

$$\mathrm{softexp}(t) = \begin{cases} e^{-t} & \text{if } t \geq 0, \\ 1 - t & \text{if } t < 0. \end{cases} \tag{8}$$

By replacing the exponential function in (1) with $\mathrm{softexp}(t)$, we expect to lower the effect of negative attenuation values and to prevent numerical instabilities. This leads to straightforward modifications of (6) and (7).

2) *Spatial regularization weights (SRW)*: there is not enough projection data to reconstruct voxels outside the FOV. Intuitively, their values should therefore be more impacted by the regularization with respect to voxels in the FOV. To realize this, we implemented regularization weights which vary according to the geometrical conditioning, formally defined by

$$\lambda_j = \frac{N_\theta}{\sum_{i=1}^{N_p} A_{ij}} \tag{9}$$

with N_θ the number of scanned views in the 360 degree axial scan configuration. The denominator represents the back-projection of a sinogram filled with ones. The number λ_j is equal to 1 in the FOV and is inversely proportional to the number of projections contributing to the voxel update. It is comparable to the scaling factor proposed by Kim et al. [5] to handle helical data with an SQS algorithm for mono-energetic data and used in their data attachment term. Instead, we make regularization stronger in regions out of the FOV. The penalization term (4) becomes

$$R_{\mathrm{SRW}}(f) = \sum_{m=1}^{N_m} \beta_m \sum_{j=1}^{N_v} \lambda_j \sum_{\xi\in\mathbb{V}_j}^{N_v} \phi(f_{mj} - f_{m\xi}). \tag{10}$$

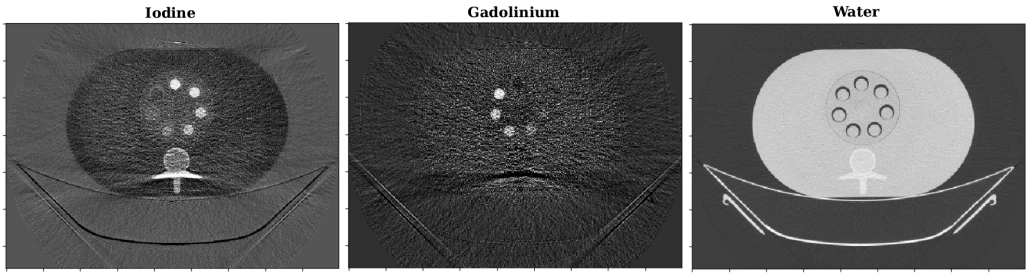

Fig. 2. Iodine, gadolinium and water maps coming from 2D reconstruction configuration. The display windows are [-5,10], [-3,7], and [-500,1500] mg/ml for iodine, gadolinium and water maps, respectively

C. Experiments

We tested the proposed solution on real spectral data of the abdomen QRM phantom acquired with an axial scan on a Philips' prototype clinical scanner recently installed in Lyon (France), which is an upgrade of [10] with mainly a larger photon counting detector. Iodine and gadolinium tubes at different concentrations were placed inside the QRM phantom. For this study, projection data were binned in 462 columns and 16 rows with 2.06 mm $\times$ 2.01 mm pixel size. The source voltage was 120 kV and 2400 views were acquired with a total 330 mA.s exposure.

The phantom was decomposed in iodine/gadolinium/water material maps. Voxel size was 1 mm $\times$ 1 mm $\times$ 3 mm. The FOV is 500 mm $\times$ 500 mm $\times$ 17.5 mm but only 450 $\times$ 330 voxels were reconstructed per slice for this object. A total of 11 slices were reconstructed, 5 central slices with only voxels in the FOV and 3 extra slices at both ends as shown in Fig. 1. The number of subsets was set to 8 and Nesterov's momentum was reset every 50 iterations (i.e. 400 voxel updates). Regularization uses a 27 voxels neighborhood. Reconstructed volumes were post-processed with an image-based correction for ring artifacts.

The material density volumes used for the non-zero initialization (NZI) were obtained with a projection-based material decomposition. The latter was calculated from a maximization of Poissonian likelihood [11] solved with 5000 iterations of the simplex algorithm of Nelder and Mead. The basis sinograms were 3D-median filtered and then reconstructed using a least squares data fidelity term and quadratic spatial regularization solved with the conjugate gradient algorithm. Voxels outside the FOV at each end were replaced from the closest ones in the FOV in the axial direction.

For comparison and to study convergence, the volume was also reconstructed in a simplified configuration. A 2D volume was reconstructed from the two middle rows of the detector averaged to form a one-row detector perfectly aligned with the source and one axial slice. This 2D axial slice was reconstructed with no subset and 1600 iterations. In this 2D configuration, we did not observe the numerical instabilities observed with the 3D configuration of Fig. 1 which is why it was used as a reference to evaluate the central slice of the 3D results (#6 in Fig. 1).

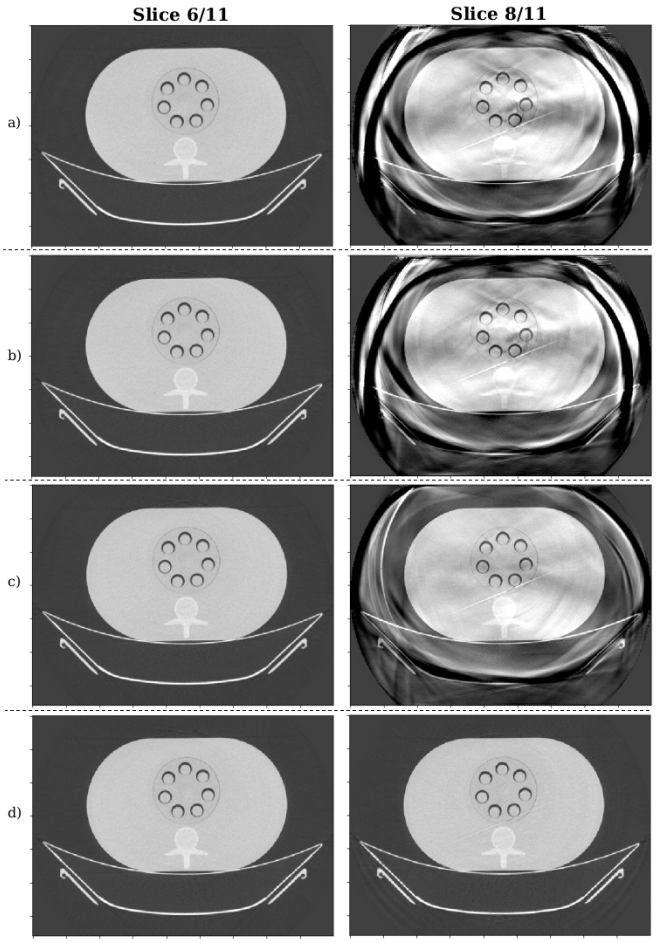

Fig. 3. Water volumes at 100 iterations, slice 6/11 is the central slice and slice 8/11 is the last top slice in FOV (cf Fig. 1. a) Uncorrected method. b) Uncorrected method with NZI. c) With Soft-E. d) With SRW. The display window is [-500,1500] mg/ml.

III. Results

The reference result is displayed in Fig. 2. The reconstruction of K-edge tubes with more than 2 mg/ml is visually satisfactory while the separation between iodine and gadolinium is subject to artifacts in the cortical part of the vertebra equivalent material.

We only show the water maps in Fig. 3, but other material decomposition images showed similar artifacts. This figure

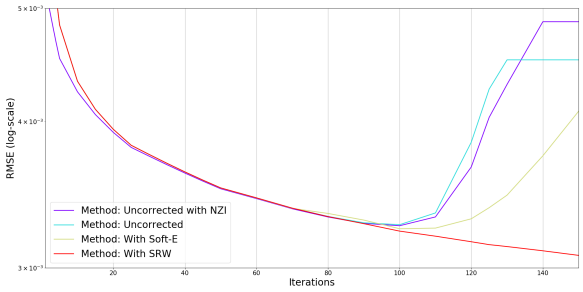

Fig. 4. RMSE between the central and the 2D volume for each methods. (Horizontal line expresses the numerical error appearance.)

corresponds to the reconstruction after 100 iterations. The process was continued until 200 iterations but faced numerical error (*not a number* (NaN) after taking the exponential of a too large number) at 130 iterations for the uncorrected method and 140 for the uncorrected method with NZI (using single precision floats). There was no such error with both the Soft-E and SRW corrections after 200 iterations. Note that we purposely chose large axial slice thickness because the numerical errors occur earlier in the iterations compared to isotropic 1 mm slice thickness but it also occurs with 1 mm slice thickness.

Fig. 3 clearly illustrates the negative effect of voxels out of the FOV and in the FOV with SQS algorithms. The NZI does not help to stabilize the behavior while the image quality with SRW is visually much more satisfactory with a minor extra computation cost. The Soft-E seems to slow down the divergent behavior of the reconstruction but cannot prevent it.

Fig. 4 shows the mean squared error between the central slice and the 2D reference volume:

$$\mathrm{RMSE} = \frac{1}{N_{vs} N_m} \sum_{j=1}^{N_{vs}} \sum_{m=1}^{N_m} \sqrt{\left(f_{bj} - f_{bj}^{2D}\right)^2} \qquad (11)$$

with N_{vs} the voxel number in a slice and f_{bj} the central slice values of each method.

Even if the central slice seems visually satisfactory after 100 iterations (Fig. 3), the RMSE reveals the divergent behavior of methods without SRW. We investigated the combination of Soft-E and SRW in the same algorithm but the contribution of adding Soft-E was negligible, both visually and on the RMSE.

The numerical instabilites outside the FOV have also been noticed without the OS implementation or the use of Nesterov's momentum technique. The SRW methods can be linked to the expression of the Hessian of the surrogate in SQS methods. This term depends on the number

$$\sum_{\xi=1}^{N_v} A_{i\xi} \qquad (12)$$

which corresponds to the projection of a volume filled with ones which appears in the SQS algorithm (7). It weights the influence of a pixel in the current update. Due to geometrical conditioning, this coefficient is smaller in voxels outside the FOV. This term is crucial to accelerate convergence in the FOV: without it, we have observed slower convergence. However, out of the FOV, it leads to larger update steps in Newton's scheme. The SRW is a simple way to preserve its effect in the FOV while guaranteeing convergence in the entire volume grid required in an iterative reconstruction.

Results were demonstrated in an axial configuration scan. We expect the helical case studied by Kim et al. [5] to be similar. The proposed correction can be applied to a helical source trajectory with a slight modification of the spatial weights λ_j.

IV. Conclusion

One-step reconstruction with an SQS algorithm leads to numerical instabilities stemming from voxels out of the FOV. Using a so-called 'soft exponential' only slightly reduces this instability at a significant computational cost. We propose to correct this effect by implementing regularization weights which balance the larger SQS update steps in voxels out of the FOV. This SRW solution is computationally efficient and preserves convergence in the FOV. It can also be used in helical scan configurations where a similar behavior is observed.

Acknowledgment

This work was performed within the framework of the EU's H2020 research and innovation program under the grant agreement No. 633937, the SIRIC LYric Grant INCa-DGOS-4664, and the LABEX PRIMES (ANR-11-LABX-0063) of Université de Lyon, within the program "Investissements d'Avenir" (ANR- 11-IDEX-0007) operated by the ANR.

References

[1] B. Chen, Z. Zhang, D. Xia, E. Y. Sidky and X. Pan, "Algorithm-enabled partial-angular-scan configurations for dual-energy CT", *Med. Phys.* vol. 45, no. 5, pp. 1857-1870, May 2018.

[2] C. Mory, B. Sixou, S. Si-Mohamed, L. Boussel and S. Rit, "Comparison of five one-step reconstruction algorithms for spectral CT", *Phys. Med. Biol.*, vol. 63, no. 23, pp. 235001, Nov. 2018.

[3] T. Weidinger, T. M. Buzug, T. Flohr, S. Kappler and K. Stierstorfer, "Polychromatic Iterative Statistical Material Image Reconstruction for Photon-Counting Computed Tomography", *International Journal of Bio. Imag.*, vol. 2016, pp. 1–15, 2016.

[4] K. Mechlem et al., "Joint statistical iterative material image reconstruction for spectral computed tomography using a semi-empirical forward model", *IEEE Trans. on Med. Imag.*, vol. 37 pp. 68-80, July 2017.

[5] D. Kim, D. Pal, J-B. Thibaul, and J. A. Fessler, "Accelerating ordered subsets image reconstruction for X-ray CT using spatially non-uniform optimization transfer", *Trans. Med. Imag.*, vol. 32, no. 11, pp. 1965–1978, Nov. 2013.

[6] S. Tilley II, W. Zbijewski and J. W. Stayman, "Model-based material decomposition with a penalized nonlinear least-squares CT reconstruction algorithm", *Phys. Med. Biol.*, vol. 64, no. 3, pp. 1-23, Jan. 2019.

[7] E. Y. Sidky, R. F. Barber, T. Gilat-Schmidt and X. Pan, "Three material decomposition for spectral computed tomography enabled by block-diagonal step-preconditioning", *Proc. 5th Int. Meeting Image Formation X-ray CT*, pp. 268-271, 2018.

[8] D. Kim, S. Ramani and J. A. Fessler, "Combining Ordered Subsets and Momentum for Accelerated X-ray CT Image Reconstruction", *Trans. Med. Imag.*, vol. 34, no. 1, pp. 167–178, Jan. 2015.

[9] A. R. De Pierro, "On the relation between the ISRA and the EM algorithm for positron emission tomography", *IEEE Trans. Med. Imag.*, vol. 12, pp. 328-333, June 1993.

[10] D P. Cormode, S. Si-Mohamed et al., "Multicolor spectral photon-counting computed tomography: in vivo dual contrast imaging with a high count rate scanner", *Sci. Rep.*, vol. 7, no. 4784, pp. 1-11, May 2017.

[11] J. P. Schlomka et al., "Experimental feasibility of multi-energy photon-counting K-edge imaging in pre-clinical computed tomography", *Phys. in Med. and Biol.*, vol. 53, no. 15, p. 4031-4047, 2008.